RSC Advances

ROYAL SOCIETY OF CHEMISTRY

www.rsc.org/advances

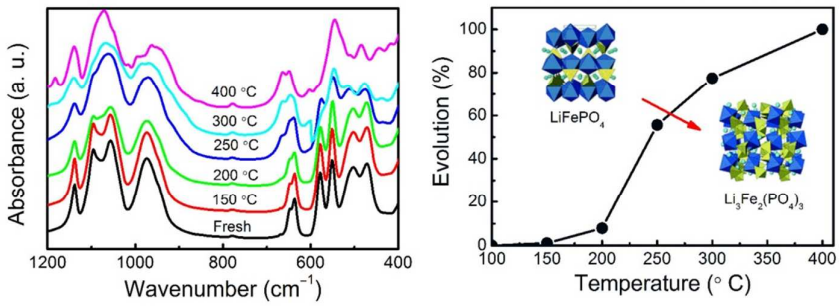

A structural evolution map of $LiFePO_4$ upon air exposure was drawn through various structural, spectroscopic, and electrochemical analyses.

Cite this: DOI: 10.1039/c0xx00000x

www.rsc.org/xxxxxx

ARTICLE TYPE

Temperature-driven structural evolution of carbon modified $LiFePO_4$ in air atmosphere

Jiangfeng Ni *[a] and Yue Wang *[b]

Received (in XXX, XXX) Xth XXXXXXXXX 20XX, Accepted Xth XXXXXXXXX 20XX
DOI: 10.1039/b000000x

Lithium iron phosphate ($LiFePO_4$) is an appealing cathode material for lithium ion batteries. However, the degradation of $LiFePO_4$ in air atmosphere presents an unavoidable challenge, due to the vulnerability of divalent Fe against oxygen attack. In this work, we carried out comprehensive research on the thermal stability and temperature-driven evolution of nanocarbon modified $LiFePO_4$ in air. The results show that $LiFePO_4$ can retain the structural stability up to 250 ˚C for short exposure to air. At long exposure, structural evolution occurs at a much lower temperature of 150 °C. The structural evolution proceeds as the temperature increases, and finishes at 400 °C. The final products are monoclinic $Li_3Fe_2(PO_4)_3$ and α-Fe_2O_3. A quantitative evolution map is drawn through electrochemical cyclic voltammetry and galvanostatic test. The results show that the major evolution takes place between 200 and 250 ˚C.

1 Introduction

Lithium iron phosphate ($LiFePO_4$) is one of the most appealing cathodes for large format lithium ion batteries (LIBs) due to its low cost, high specific capacity, excellent cycling performance, and superior safety.[1, 2] These merits is inherently rooted in its olivine structure. Olivine $LiFePO_4$ crystallizes in the orthorhombic structure, in which oxygen atoms form slightly distorted hexagonal close-packed arrangement, and both Li atom and Fe atom take the octahedral sites. The PO_4 polyanion enhances the redox potential of Fe^{2+}/Fe^{3+} to 3.4 V (vs. Li, unless otherwise stated) via an inductive effect, but also prevents the possible oxygen release in abused condition.[3] However, the low electronic (~10^{-9} S cm^{-1}) and the resulting sluggish kinetics present a significant challenge for the scalable utilization of $LiFePO_4$. To address this issue, numerous strategies have been proposed and shown promising prospect during the last decades. These strategies include surface modification,[4] nanocarbon wiring,[5, 6] ion doping,[7, 8] size reduction,[9] shape tuning,[10] and so forth.

Generally, reduction of particle size could efficiently mitigate the kinetic issues of $LiFePO_4$.[11, 12] However, fine $LiFePO_4$ materials are sensitive to air exposure, due to large surface area and high activity.[13] This presents a significant challenge for storage and processing of $LiFePO_4$ materials, when the materials are highly possible to be exposed to air at higher ambient temperature. Previously, Martin et al. reported that air exposure of $LiFePO_4$ at 120°C could lose 2.3% of lithium (oxidation of $LiFePO_4$).[14] Certainly, this evolution would be more serious at higher temperatures. Therefore, it is essential to probe the thermal evolution process of $LiFePO_4$ versus ambient temperatures, particularly at temperature above room temperature. Nonetheless, such a issue has barely been addressed so far.

In this work, the evolution of $LiFePO_4$ materials in air as a function of ambient temperature was examined. Carbon coated $LiFePO_4$ was applied as the starting material as carbon modification is currently popular for olivine materials. A series of air-exposed $LiFePO_4$ derivatives at different temperatures were prepared. These materials were systematically investigated using various structural, spectroscopic, and electrochemical analyses. Analysis on these results could enable us to draw a clear map of temperature-driven evolution of $LiFePO_4$ in air.

2 Experimental

Carbon coated $LiFePO_4$ materials were prepared via solid-state reaction from Li_2CO_3, $Fe(II)C_2O_4{\cdot}2H_2O$ and $NH_4H_2PO_4$ and sucrose. The final product was predicted to contain 1 wt% carbon. Details of the experimental can be found in the supporting information (ESI). Thermal evolution of $LiFePO_4$ materials was probed in two approaches. One is to collect thermogravimetric analysis (TGA) data on a SDT 2960 apparatus (TA Instruments). The other is to hold $LiFePO_4$ materials in different temperatures, and then to characterize these derivatives using by chemical and electrochemical analyses.

3 Results and discussion

The structure of the $LiFePO_4$ is identified by XRD and Rietveld refinement (Figure S1). The XRD pattern can be fully indexed to be olivine structure (JCPDS No. 81-1173) without diffraction peaks due to impurity. Rietveld analysis on the XRD data reveals lattice parameters to be a = 1.0316(2) nm, b = 0.6002 (3) Å, c = 0.4690(3) Å, and V= 0.2904 nm^3, in line with previous results.[3, 15] This result implies that the olivine phase has been readily fabricated through the solid route.

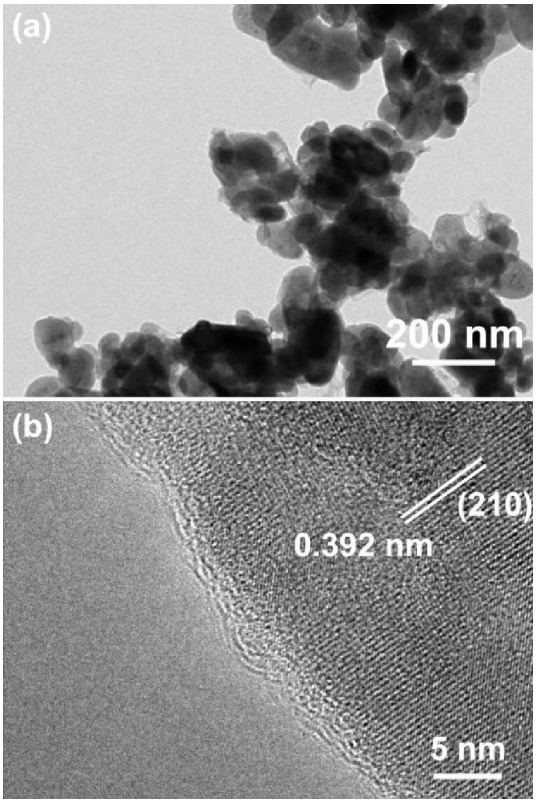

Figure 1. Morphology of the prepared $LiFePO_4$. (a) TEM and (b) high resolution TEM images. The lattice fringe spacing of 0.392 nm shown in (b) coincides with the (210) facets of olivine $LiFePO_4$.

Figure 1 illustrates the TEM images of the $LiFePO_4$, revealing that most grains are in the nanoscale with average particle size of 100 nm. An amorphous nanolayer covered on the particles can be clearly observed, which is identified as carbon derived from sucrose (Figure 1a). The thickness of carbon nanolayer is only about 2 nm (Figure 1b) due to a low carbon loading, but it remarkably enhances the material conductivity to 2×10^{-2} S cm^{-1}.

The thermal evolution of $LiFePO_4$ in air atmosphere was examined by TGA, and the result is presented in Figure 2. The data were collected from room temperature to 700 ˚C at a ramping rate of 10 ˚C min^{-1}. Mass changes reflecting possible phase evolution can be readily seen from the TGA curve. There are two possible reactions involved in the heating process. One is the oxidation of $LiFePO_4$ (Eq.1), and the other the burning out of coated carbon (Eq. 2).[16] In detail, the mass loss of 0.4 wt% below 150 ˚C is due to the removal of adsorption water. From 150 to 250 ˚C, the mass remains constant (inset in Figure 2), suggesting that the $LiFePO_4$ is still stable in air at this temperature range. From 250 to 400 ˚C, gradual mass augment suggests possible oxygen uptake due to oxidation of divalent Fe species (Eq.1). Interestingly, this mass then remains steady in the following temperature range of 400–450 ˚C. However, this is probably because the mass gain and loss between $LiFePO_4$ oxidation and carbon loss (Eq. 2) reach a balance. Above 450 ˚C, most amorphous carbon is burnt out and bulk oxidation of divalent Fe occurs, leading to a net mass gain of 3.6 wt%. As a full oxidization of $LiFePO_4$ (Eq. 1) results in a mass gain of 5.1 wt%, the exact carbon loading in the $LiFePO_4$ product is 1.1 wt% .

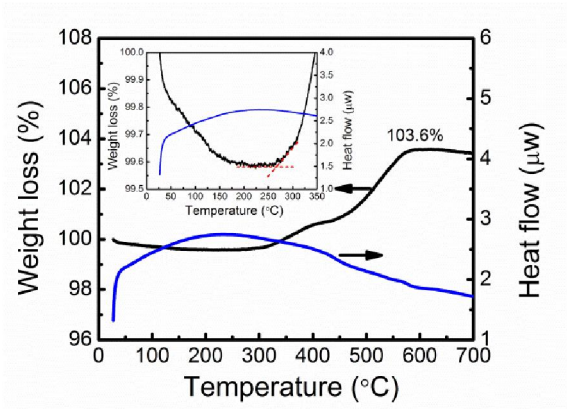

Figure 2. TGA curves of $LiFePO_4$ in air atmosphere at ramping rate of 10 ˚C min^{-1}. Inset shows the enlarged curve before 350 ˚C.

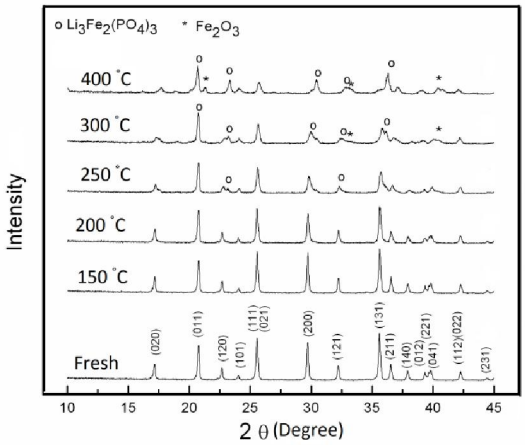

Figure 3. Evolution of XRD patterns of $LiFePO_4$ exposed to air versus temperature. The $LiFePO_4$ samples were held at set temperatures for 3 h.

$$6LiFePO_4 + 3/2O_2 \rightarrow 2\ Li_3Fe_2(PO_4)_3 + Fe_2O_3 \quad \text{(Eq. 1)}$$

$$C + O_2 \rightarrow CO_2 \quad \text{(Eq. 2)}$$

To investigate the structural evolution under long exposure to air, the $LiFePO_4$ samples were held at set temperatures (150–400 ˚C) for 3 h. These derivatives were then subject to structural, spectroscopic and electrochemical analyses to reveal the evolution process. XRD patterns of these $LiFePO_4$ products are shown in Figure 3. It is clearly seen from Figure 3 that degradation of the olivine phase starts at 200 ˚C. At this temperature, the diffraction intensity decreases and splitting of the (020) peak in the pattern occurs. When the temperature increases to 250 ˚C, new diffraction peaks due to monoclinic $Li_3Fe_2(PO_4)_3$ [17] and α-Fe_2O_3 [18] appear in the pattern of the derivative. This result indicates that bulk phase evolution due to oxygen uptake occurs. Further increasing the temperature to 300 ˚C results in more $Li_3Fe_2(PO_4)_3$ and Fe_2O_3 phases at the expense of olivine structure. When the $LiFePO_4$ was treated at 400 ˚C, no peaks due to olivine phase can be detected in the XRD pattern, suggesting a complete structural evolution.

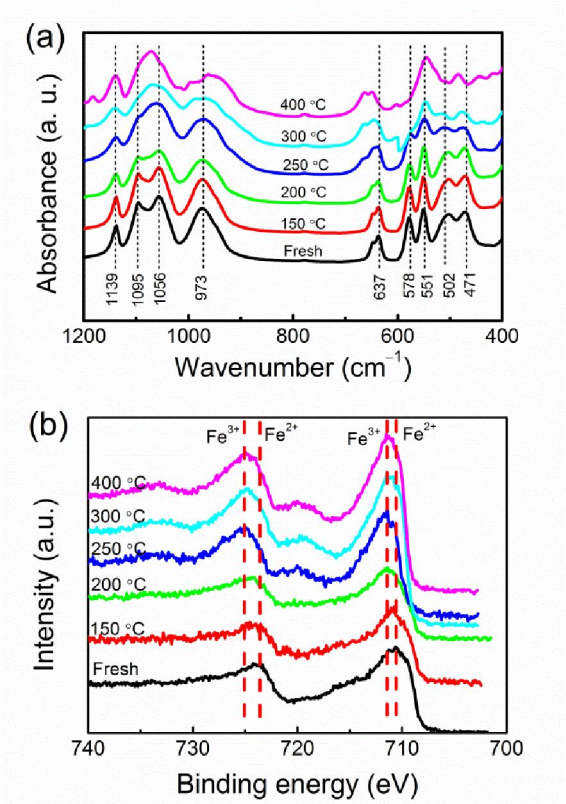

Figure 4. Evolution of (a) FTIR and (b) XPS spectra of $LiFePO_4$ exposed to air upon heating at various temperatures.

In addition to XRD, the temperature-driven structural evolution of the $LiFePO_4$ was further studied by FTIR. It is known that $LiFePO_4$ has two kinds of vibrational motions in the FTIR: internal modes originating from intramolecular vibrations of PO_4 polyanion and external mode due to lattice vibration.[19] The latter involving Li ion motion usually occurs below 400 cm^{-1} and is difficult to discern, thus will not be discussed here. As shown in Figure 4a, the fresh $LiFePO_4$ exhibits four absorption bands at 1139, 1095, 1056, and 973 cm^{-1}, which can be assigned to sketching of PO_4 group. Five additional bands at 637, 578, 551, 502 and 471 cm^{-1} can be ascribed to the bending mode of PO_4 group.[20] The derivative treated at 150 ˚C shows a quite similar spectrum as the fresh $LiFePO_4$ and imply an intact microstructure, consistent with the XRD result. However, structural evolution can be clearly observed for the sample heated at 200 ˚C. In this spectrum, the sketching bands of PO_4 group become broad and the band at 1095 cm^{-1} loses its intensity to a large degree. Pronounced evolution is visible in the spectrum of the sample treated at 250 ˚C. The band at 1095 cm^{-1} disappears and two new bands at 668 and 437 cm^{-1} appear, which might be ascribed to α-Fe_2O_3.[21] Further raising the temperature to 300 and 400 ˚C results in disappearance of more absorption bands ascribed to olivine phase. This is accompanied with emerging of new absorption bands located at 1182, 962, 602 cm^{-1}, which can be related to monoclinic $Li_3Fe_2(PO_4)_3$.

As oxidation of divalent Fe triggers the structural evolution of olivine phase, XPS spectroscopy was recorded to probe the evolution of chemical valence of Fe in $LiFePO_4$. XPS is a typical surface technique with high sensitivity, thus it would give direct evidence of structural evolution. Figure 4b shows the XPS spectra of Fe 2P for the LiFePO4 and derivatives. The peaks at 710.5 eV and 723.6 eV for the fresh $LiFePO_4$ can be assigned, respectively, to Fe $2P_{3/2}$ and Fe $2P_{1/2}$ in the divalent state.[22, 23] A shift of Fe 2P peaks to higher binding energy is observed for the heated derivatives, indicating that divalent Fe species in the surface are readily oxidized even at 150 ˚C. For the derivatives exposed to a temperature of 200 ˚C or above, the Fe $2P_{3/2}$and $2P_{1/2}$ peaks shift to higher binding energy of 711.5 eV and 725.2 eV, respectively. This shift in combination of occurrence of two shoulder peaks at 719.8 eV and 732.7 eV proves that the divalent Fe has transformed to the trivalent.[22] It is worth noting that this temperature is lower than those obtained by XRD and FTIR, because XPS is more sensitive to surface change and evolution of Fe species probably initiates from the surface of grains.

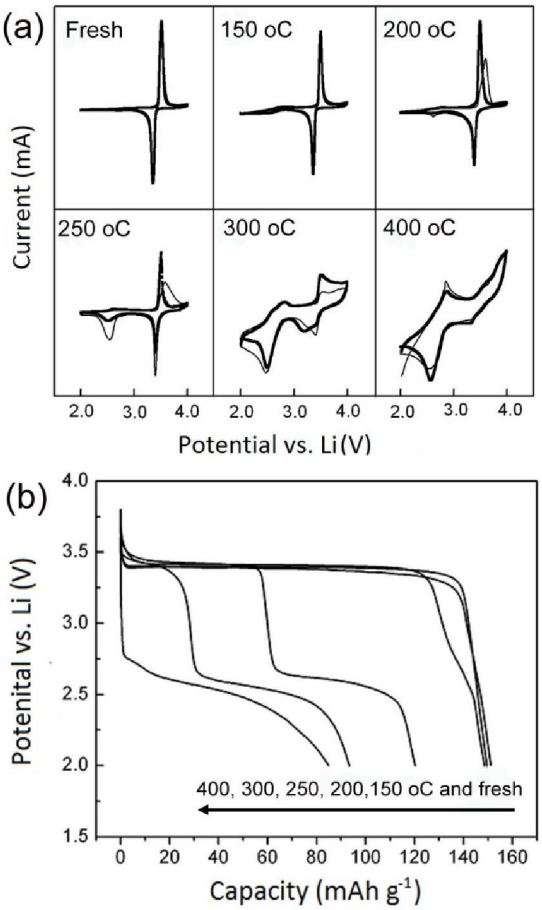

Figure 5. (a) CV graphs and (b) discharge curves of $LiFePO_4$ exposed to air upon heating at various temperatures.

The XRD and FTIR results suggest that evolution of $LiFePO_4$ bulk initiates at 200˚C, while the XPS suggest that the surface degradation starts at a lower temperature of 150˚C.[14] To understand this evolution from the viewpoint of electrochemistry, CV and galvanoststic tests on the $LiFePO_4$ samples were implemented. Figure 5a displays their CV curves in the first two cycles at a scanning rate of 0.1 mV s^{-1}. The fresh $LiFePO_4$ discloses a distinct redox pairs at 3.4 V, representing the typical Fe^{2+}/Fe^{3+} redox reaction in olivine.[1, 24] This reaction reveals a

considerable reversibility, due to small particle size of $LiFePO_4$ and uniform carbon coating.[25, 26] Surprisingly, the CV curve is highly sensitive to structural evolution. A redox pair emerges at 2.7 V for the $LiFePO_4$ upon 150 ˚C exposure, unambiguously reflecting the occurrence of structural evolution at this temperature. The 2.7 V peak can be ascribed to Li insertion/extraction in the monoclinic $Li_3Fe_2(PO_4)_3$.[27] This redox pair continues growing with increasing exposing temperature, at the expense of the original 3.4 V pair. Finally, the peaks at 3.4 V disappears for the 400 ˚C sample, and only the 2.7 V redox remains, suggesting a full evolution of $LiFePO_4$ phase.[28] This CV results correlate the structural and spectroscopic analyses well.

Figure 5b shows their galvanostatic discharge curves during the first cycle. The fresh $LiFePO_4$ delivers a reversible capacity of ~150 mAh g^{-1} with flat potential plateau at 3.4 V, indicating favorable electrochemical activity of olivine material.[8] Similarly, slight changes in the end of discharge can be found for the $LiFePO_4$ exposed to air at 150 ˚C. This change becomes remarkable for the samples treated at 200 ˚C or higher temperatures, and a new potential at 2.7 V appears. The new plateau matches the CV peak at 2.7 V, and can be due to Li insertion into the monoclinic $Li_3Fe_2(PO_4)_3$ phase. Theoretically, the $Li_3Fe_2(PO_4)_3$ can electrochemically accommodate two Li ions per formula unit, leading to a capacity of 128 mAh g^{-1}.[27] Increasing the exposure temperature results in reduction of the 3.4-V plateau and concomitant increase of the 2.7-V one monotonically. The $LiFePO_4$ derivative at 400 ˚C only exhibits one plateau at 2.7 V, indicating the entire loss of olivine phase. Meanwhile, the overall discharge capacity decreases with increasing temperature, probably due to the lower capacity of the monoclinic phase and the gradual loss of conductive network of carbon. If ignoring the kinetic factor, we can quantitatively draw an evolution map by comparing the length of the two plateaux (Figure S2, ESI). The results reveal that the thermal evolution starts at 150 ˚C and the major process takes place between 200 and 250 ˚C. Previously, Martin et al reported a 2.3% evolution of $LiFePO_4$ at a lower temperature of 120 ˚C.[14] The discrepancy might stem from the carbon coating. During the synthesis, we added sucrose rather than carbon as Martin et al. did in their case, to form a composite. This in situ carbon coating process forms an uniform overlayer on the surface of $LiFePO_4$ particles and thus provide good protection from oxygen attack,[29-31] which can significantly retard the structural evolution.

4 Conclusions

The temperature-driven evolution of the carbon coated $LiFePO_4$ in air atmosphere was investigated using various structural, spectroscopic and electrochemical techniques. The results indicate that nanocarbon coated $LiFePO_4$ is stable up to 250 ˚C over short exposure to air. Under long exposure, however, the bulk phase stability can maintain at 200˚C while the surface evolution initiates at a much lower temperature of 150 ˚C, as revealed by XRD, FTIR, XPS and electrochemical analyses. Structural evolution proceeds as the temperature increases, and the final products includes monoclinic $Li_3Fe_2(PO_4)_3$ and α-Fe_2O_3. The evolution process can be quantitatively drawn through electrochemical galvanostatic test. The results show that the major evolution takes place between 200 and 250 ˚C. This research provides quantitative understanding on the temperature-driven evolution of olivine $LiFePO_4$ materials in air, and surely will benefit relative material research and production. [32-34]

Acknowledgments

Support of this work by National Natural Science Foundation of China (51302181), China Postdoctoral Science Foundation (2014M551647), and SRF for ROCS, SEM is acknowledged.

Notes and references

[a] *College of Physics, Optoelectronics and Energy, Soochow University, Suzhou 215006, China. Fax: +81-512-67875503; Tel: +81-512-67875503; E-mail: jeffni@suda.edu.cn (J. Ni)*
[b] *Institute of Chemical Defense of PLA, Beijing 102205, China. E-mail: wyuejms52088@sohu.com (Y. Wang)*

† Electronic Supplementary Information (ESI) available: [Materials synthesis and chracterization, electrochemical evalution, and evolution of $LiFePO_4$]. See DOI: 10.1039/b000000x/

1. A. K. Padhi, K. S. Nanjundaswamy and J. B. Goodenough, *J. Electrochem. Soc.*, 1997, **144**, 1188-1194.
2. M. S. Whittingham, *Chem. Rev.*, 2014, **114**, 11414-11443.
3. C. Hu, Y. Wu and Y. Dai, *Funct. Mater. Lett.*, 2014, **07**, 1450016.
4. M. Molenda, A. Chojnacka, M. Bakierska and R. Dziembaj, *Mater. Technol.*, 2014, **29**, A88-A92.
5. J. W. Zhang, L. H. Zhuo, L. L. Zhang, C. Y. Wu, X. B. Zhang and L. M. Wang, *J. Mater. Chem.*, 2011, **21**, 6975-6980.
6. J. F. Ni, Y. H. Han, L. J. Gao and L. Lu, *Electrochem. Commun.*, 2013, **31**, 84-87.
7. J. F. Ni, H. H. Zhou, J. T. Chen and X. X. Zhang, *Chinese Journal of Inorganic Chemistry*, 2005, **21**, 472-476.
8. J. Ni, Y. Zhao, J. Chen, L. Gao and L. Lu, *Electrochem. Commun.*, 2014, **44**, 4-7.
9. J. F. Ni, M. Morishita, Y. Kawabe, M. Watada, N. Takeichi and T. Sakai, *J. Power Sources*, 2010, **195**, 2877-2882.
10. C. Nan, J. Lu, C. Chen, Q. Peng and Y. Li, *J. Mater. Chem.*, 2011, **21**, 9994.
11. L. X. Yuan, Z. H. Wang, W. X. Zhang, X. L. Hu, J. T. Chen, Y. H. Huang and J. B. Goodenough, *Energy Environ. Sci.*, 2011, **4**, 269-284.
12. C. Gong, F. Deng, C.-P. Tsui, Z. Xue, Y. S. Ye, C.-Y. Tang, X. Zhou and X. Xie, *J. Mater. Chem. A*, 2014, **2**, 19315-19323.
13. Y. G. Wang, P. He and H. S. Zhou, *Energy Environ. Sci.*, 2011, **4**, 805-817.
14. J. F. Martin, A. Yamada, G. Kobayashi, S. Nishimura, R. Kanno, D. Guyomard and N. Dupré, *Electrochem. Solid-State Lett.*, 2008, **11**, A12-A16.
15. P. F. Xiao, B. Ding, M. O. Lai and L. Lu, *J. Electrochem. Soc.*, 2013, **160**, A918-A926.
16. I. Belharouak, C. Johnson and K. Amine, *Electrochem. Commun.*, 2005, **7**, 983-988.
17. M. Morcrette, C. Wurm and C. Masquelier, *Solid State Sci.*, 2002, **4**, 239-246.

18. X.-L. Cheng, J.-S. Jiang, M. Hu, G.-Y. Mao, Z.-W. Liu, Y. Zeng and Q.-H. Zhang, *CrystEngComm*, 2012, **14**, 3056-3062.
19. C. M. Burba and R. Frech, *J. Electrochem. Soc.*, 2004, **151**, A1032-A1038.
20. J. F. Ni, Y. H. Han, J. Z. Liu, H. B. Wang and L. J. Gao, *ECS Electrochem. Lett.*, 2013, **2**, A3-A5.
21. G. H. Jiang and J. S. Jiang, *Chem. J. Chin. Univ.*, 2004, **25**, 405-408.
22. M. Descostes, F. Mercier, N. Thromat, C. Beaucaire and M. Gautier-Soyer, *Appl. Surf. Sci.*, 2000, **165**, 288-302.
23. K. Shimoda, H. Sugaya, M. Murakami, H. Arai, Y. Uchimoto and Z. Ogumi, *J. Electrochem. Soc.*, 2014, **161**, A1012-A1018.
24. Z.-X. Chi, W. Zhang, X.-S. Wang, F.-Q. Cheng, J.-T. Chen, A.-M. Cao and L.-J. Wan, *J. Mater. Chem. A*, 2014, **2**, 17359-17365.
25. J. Yang, J. Wang, Y. Tang, D. Wang, B. Xiao, X. Li, R. Li, G. Liang, T.-K. Sham and X. Sun, *J. Mater. Chem. A*, 2013, **1**, 7306-7311.
26. B. Ding, G. Ji, Y. Ma, P. Xiao, L. Lu and J. Y. Lee, *J. Power Sources*, 2014, **247**, 273-279.
27. H. Karami and F. Taala, *J. Power Sources*, 2011, **196**, 6400-6411.
28. D. L. Smiley, L. J. Davis and G. R. Goward, *J. Phys. Chem. C*, 2013, **117**, 24181-24188.
29. K. Weichert, W. Sigle, P. A. van Aken, J. Jamnik, C. Zhu, R. Amin, T. Acartuerk, U. Starke and J. Maier, *Journal of the American Chemical Society*, 2012, **134**, 2988-2992.
30. J. F. Ni, L. J. Gao and L. Lu, *J. Power Sources*, 2013, **221**, 35-41.
31. J. Ni, L. Zhang, S. Fu, S. Savilov, S. Aldoshin and L. Lu, *Carbon*, 2015, **92**, 15–25.
32. J. Wang, J. Yang, Y. Zhang, Y. Li, Y. Tang, M. N. Banis, X. Li, G. Liang, R. Li and X. Sun, *Adv. Funct. Mater.*, 2013, **23**, 806-814.
33. J. Wang, Y. Tang, J. Yang, R. Li, G. Liang and X. Sun, *J. Power Sources*, 2013, **238**, 454-463.
34. J. Wang, J. Yang, Y. Tang, J. Liu, Y. Zhang, G. Liang, M. Gauthier, Y. K. Chen-Wiegart, M. Norouzi Banis, X. Li, R. Li, J. Wang, T. K. Sham and X. Sun, *Nat. Commun.*, 2014, **5**.